CORROSION SCIENCE AND TECHNOLOGY, Vol.24, No.5(2025), pp.327~346 pISSN 1598-6462 / eISSN 2288-6524
[Research Paper] DOI: https://doi.org/10.14773/cst.2025.24.5.327

Advanced Bipolar Model Based on the Semiconductive Properties of the Passive Film in Stainless Steel

Seung-Heon Choi[1], Young-Ran Yoo[2], Young-Cheon Kim[1,3,†], and Young-Sik Kim[3]

[1]*Department of Materials Science and Engineering, Gyeongkuk National University, 1375 Gyeongdong-ro, Andong 36729, Republic of Korea*
[2]*Department of Semiconductor Facilities, Gumi Campus of Korea Polytechnics, 84, Suchul-Daero 3-Gil, Gumi 39257, Republic of Korea*
[3]*Materials Research Centre for Energy and Clean Technology, Gyeongkuk National University, 1375 Gyeongdong-ro, Andong 36729, Republic of Korea*

(Received October 14, 2025; Revised October 27, 2025; Accepted October 27, 2025)

This study evaluated the electrochemical and semiconductive properties of passive films on austenitic stainless steels with varying pitting resistance equivalent (PRE) values in deaerated HCl solutions. The electrochemical analysis indicated that higher PRE values resulted in a lower passive current density (i_p) and an increased polarization resistance (R_p). XPS depth profiling showed that the passive film had a bilayer structure: the inner layer primarily consisted of Cr_2O_3 / $Cr(OH)_3$, while the outer layer was enriched with oxyanion species such as CrO_4^{2-} and MoO_4^{2-}. As PRE increased, the proportion of Cr_2O_3 in the inner layer rose, while the outer layer had a higher concentration of oxyanions. These alterations led to a simultaneous increase in both p-type and n-type slopes. To quantify this effect, the 'Bipolar Index (|p-type slope| + |n-type slope|)' was applied, and an advanced bipolar model of the passive film was proposed. An increase in the bipolar index was associated with a decrease in passive current density (i_p), an increase in polarization resistance (R_p), and a reduction in the total defect density within the passive film.

Keywords: *Stainless steel, Passive film, PRE, Mott-Schottky, Advanced bipolar model*

1. Introduction

Stainless steel is an iron-based alloy containing more than 13 wt% chromium (Cr), and its excellent corrosion resistance is attributed to the formation of a thin, stable oxide film on the alloy surface when exposed to air or corrosive environments [1-4]. Owing to these properties, stainless steels are widely utilized in industrial fields such as power plants and marine structures. In highly aggressive corrosive environments, they are considered more promising structural materials than carbon steels. The corrosion resistance of stainless steel is determined by the passive film. This passive film forms at the nanometer scale between the metal substrate and the corrosive environment, blocking the leaching of metal ions and the penetration of external aggressive ions (such as Cl^- and SO_4^{2-}) [5,6].

The passive film is formed at a specific potential, leading to a sharp decrease in the current density of the metal. Since the early 20th century, the formation of passive films has been explained by various theories, among which the "oxide film theory" is one of the most representative [7]. This theory proposes that the metal is oxidized and reaction products, such as metal oxides or other compounds, form an oxide film on the surface, thereby protecting the metal. Another representative theory is the "adsorption theory" [8]. This theory suggests that anions in the solution (e.g., OH^-, O^{2-}) are selectively adsorbed onto the metal surface, forming a passive film that protects the metal. These theories have played a fundamental role in explaining the existence of passive films and their basic protective mechanisms.

However, the actual passive film is not merely a simple oxide layer but rather a more elaborate structure in which electronic structure, ion distribution, and electrochemical properties are intricately linked. Accordingly, as research has advanced, more sophisticated theories have been

[†]Corresponding author: yckim@gknu.ac.kr
Seung-Heon Choi: Ph.D. Candidate, Young-Ran Yoo: Professor, Young-Cheon Kim: Professor, Young-Sik Kim: Emeritus

proposed, such as "Electron Configuration Induced Adsorption Passivity," [9] which explains the formation and stabilization of passive films through orbital interactions between metals and adsorbed species, and "Ion Space Charge Induced Passivity," [10] which interprets the electrochemical properties of passive films in terms of ion distribution and the formation of electrical space charges within the film [11]. These theories have been instrumental in explaining various electrochemical phenomena, including the stability of passive films, their semiconductive properties, and the formation of the electric double layer. Based on these formation mechanisms, the composition of the passive film was investigated using XPS. Several studies have reported that the passive film on stainless steel is divided into two layers. The inner layer at the metal/film interface is mainly composed of Cr enriched oxides, while the outer layer consists of Fe-based oxides or metal hydroxides [12-17].

The passive film on stainless steel is generally regarded as a bilayer structure, and several studies have focused on the formation of an electric field within the film, employing photocurrent measurements and capacitance-based Mott–Schottky analysis. Through these approaches, it has been interpreted that the passive film exhibits semiconductive properties. Based on such analyses, the major theories concerning the passive film on stainless steel can be broadly categorized into two types. The first is the point defect model proposed by Hoar [18], which explains the growth and breakdown of oxide films through the migration of metal and oxygen ion vacancies, and it has been widely applied in the analysis of corrosion resistance [19]. The second is the bipolar fixed charge model introduced by Sakashita and Sato [20-22], which describes the tendency of ion selectivity (cationic or anionic) within the film depending on alloying elements such as Cr and Mo [23-27]. Based on these two theories, Mott–Schottky analysis has demonstrated that stainless steels can form n-type [28-31], or p–n type [32-36] passive films depending on potential variations or environmental conditions.

The pitting resistance equivalent (PRE), calculated from the chemical composition, is an index used to predict the resistance of stainless steels to localized corrosion. The major contributing elements are Cr, Mo, W, and N. Pitting corrosion in stainless steels occurs when the material is exposed to aggressive environments such as chloride ions (Cl^-), and the formation of a stable passive film is critical to suppress it. The elements included in the PRE formula directly influence the composition, structure, and electrochemical properties of the passive film, and these changes contribute to the improvement of pitting resistance [37-40].

Cr has been reported to improve corrosion resistance by promoting the formation of a dense Cr_2O_3 layer in the inner part of the passive film, thereby enhancing its p-type semiconductive properties [28,41-43]. In addition, while Cr plays a dominant role in the initial formation of the passive film, Mo is known to promote its reformation and stabilization. This has been reported to enhance corrosion resistance primarily by strengthening the metal–oxygen bond through the action of MoO_4^{2-} and improving the structural stability of the passive film [44-47]. W has been reported to behave similarly to Mo, existing in the form of WO_3 or WO_4^{2-} ions, which enhance the stability of the passive film and contribute to long-term improvement of corrosion resistance [48,49].

As described above, numerous studies have reported that alloying elements such as Cr, Mo, and W influence the corrosion resistance and semiconductive properties of passive films. However, most of these studies have been limited to analyzing the resistance or point defect density of passive films in stainless steels with different PRE grades. In other words, previous studies have mainly focused on evaluating corrosion resistance as a function of PRE, while only limited efforts have been made to distinguish the semiconductive properties of passive films formed under various environments and to interpret them in connection with corrosion resistance.

The conventional bipolar model [20-25] categorizes the passive film into a Cr_2O_3 rich inner layer, a $Cr(OH)_3$ rich intermediate layer, and an outermost layer containing metal oxyanions (MeO_4^{2-}) such as CrO_4^{2-} and MoO_4^{2-}. However, this model has limitations in adequately reflecting the diverse distribution of components within the passive film. In particular, in the outer layer, OH^-, adsorbed H_2O species, and metal hydroxides occupy significant fractions, while in the inner layer, oxides of Fe and Mo coexist alongside Cr oxides. Despite this, the conventional model oversimplifies the structure by attributing each region to a single representative species, resulting in insufficient explanation of the correlation with

actual electrochemical behavior. Moreover, it does not provide a clear description of how the p-type and n-type characteristics observed in Mott–Schottky analysis are formed and reinforced [20-25].

Therefore, in this study, the corrosion resistance of austenitic stainless steels was evaluated based on PRE. The semiconductive properties of passive films formed under various corrosive environments were analyzed using Mott–Schottky and electrochemical methods. Finally, the correlation between the semiconductive structure of the passive films and their corrosion resistance was compared and analyzed.

2. Experimental Methods

2.1 Materials

The stainless steels used in this study were prepared using high-purity Fe, Cr, Ni, Mo, Fe-Cr-N, Fe-Si, Fe-Mn, and other alloying constituents. After melting in a high-frequency vacuum induction furnace, the ingots were processed into 6 mm plates by hot rolling. The hot-rolled specimens were then cut into appropriate sizes depending on the purpose of use and subjected to annealing heat treatment at 1175 ºC for 30 min. Table 1 presents the results of the compositional analysis of the test alloys.

2.2 polarization test

To evaluate the corrosion and passivation behavior of stainless steels with different PRE values in hydrochloric acid environments, polarization tests were conducted. The specimens were cut into dimensions of 1.2 cm × 1.2 cm, and a rubber coated copper wire was spot-welded onto one side of each specimen to ensure electrical contact. The specimens were then mounted with epoxy resin. The exposed surface was mechanically polished using SiC papers ranging from #80 to #2000, after which all areas except for a 1 cm^2 exposure area were coated with epoxy. Polarization tests were performed using a potentiostat (Interface 1000, Gamry Instruments, Warminster, PA, USA). A saturated calomel electrode(SCE) was used as the reference electrode, and platinum was employed as the counter electrode. To examine the effect of hydrochloric acid concentration, test solutions of 0.1 N, 0.5 N, and 1.0 N HCl were prepared. All experiments were conducted of 25 ºC. Prior to testing, the solutions were deaerated by purging with nitrogen gas at a flow rate of 250 mL/min for 30 min. The polarization scans were initiated from potential 0.1 V more negative than the corrosion potential (E_{corr}) and continued up to the oxygen evolution potential at a linear scan rate of 0.33 mV/s [51].

2.3 AC impedance test

To evaluate the passivation behavior of stainless steels with different PRE values in hydrochloric acid environments, AC impedance measurements were carried out. The specimens and test solutions were prepared under the same conditions as those used for the polarization tests. The AC impedance tests were conducted using a potentiostat (Interface 1000, Gamry Instruments, Warminster, PA, USA). Passive films were first formed for 2 h at a potential of +0.6 V(SCE), where stable passivation was commonly observed from the polarization tests, and the impedance spectra were subsequently measured while maintaining the same potential. The frequency range was set from 10 kHz to 0.1 Hz, and the polarization resistance (R_p) was determined by fitting the data to the Randles model [45].

2.4 XPS analysis

For XPS analysis, the specimens were sequentially polished with SiC papers (#80 to #2000) and subsequently mirror-polished using 3 μm diamond paste. They were then ultrasonically cleaned in ethyl alcohol, dried, and immersed in deaerated hydrochloric acid solution prepared by purging nitrogen gas (N_2, 100 mL/min) for 30 min. Passive films were formed at +0.6 V(SCE) for 2 h

Table 1. Chemical compositions of austenitic stainless steels

Alloy	Cr	Ni	Mo	Mn	Si	P	S	C	Cu	N	Fe	PRE_{30}
904L	20.8	23.4	4.4	1.6	0.6	0.005	0.004	0.01	1.5	-	Bal.	35.3
AL-6X	21.3	23.2	5.9	0.9	0.6	0.007	0.004	0.01	0.05	-	Bal.	40.7
SR-50A	22.8	22.6	6.1	0.4	0.3	0.03	0.001	0.02	0.1	0.24	Bal.	50.3

PRE_{30} = %Cr + 3.3(%Mo + 0.5%W) + 30%N

using a potentiostat (Interface 1000, Gamry Instruments, Warminster, PA, USA), after which the specimens were stored in a sealed container under a nitrogen atmosphere to minimize surface contamination. XPS measurements were performed using a K-Alpha instrument (Thermo UK, Altrincham, UK) with Al Kα radiation (1486.6 eV, 12 kV, 3 mA) as the X-ray source. Depth profiling was carried out by Ar ion sputtering (1 kV, 2 μA), and the same conditions were applied for surface pretreatment. The collected spectra were analyzed using Avantage software (Version 6.8.1.4, Thermo Fisher Scientific, Waltham, MA, USA). The C 1s peak was calibrated to 284.6 eV, and deconvolution was applied to each elemental peak to identify oxidation states and chemical species.

2.5 Mott-Schottky analysis

To evaluate the semiconductive properties of austenitic stainless steels with different PRE values, Mott–Schottky analysis was performed. The specimens and test solutions were prepared under the same conditions as those used for the polarization tests. Passive films were formed at +0.6 V(SCE) for 2 h using a potentiostat (Interface 1000, Gamry Instruments, Warminster, PA, USA). After film formation, capacitance measurements were conducted for Mott–Schottky analysis with an AC amplitude of 10 mV (peak-to-peak) and a frequency of 1,580 Hz. The potential range was set between +1.0 V(SCE) and −1.0 V(SCE) at a scan rate of 20 mV/s, ensuring that the passive film was not damaged during measurement. The permittivity (ε) used in the N_A and N_D calculations was set to 15.6, a value commonly used for stainless steel [36,37,48]. The vacuum permittivity ($\varepsilon_0 = 8.854 \times 10^{-12}$ F/m) and the elementary charge ($e = 1.602 \times 10^{-19}$ C) were also used in the calculations. The flattening potential (E_{fb}), donor density (N_D), and acceptor density (N_A) were determined from the Mott–Schottky curve [28].

3. Results

3.1 Effect of PRE on the electrochemical properties of stainless steels

Fig. 1 shows the polarization behavior (Fig. 1a–c) and

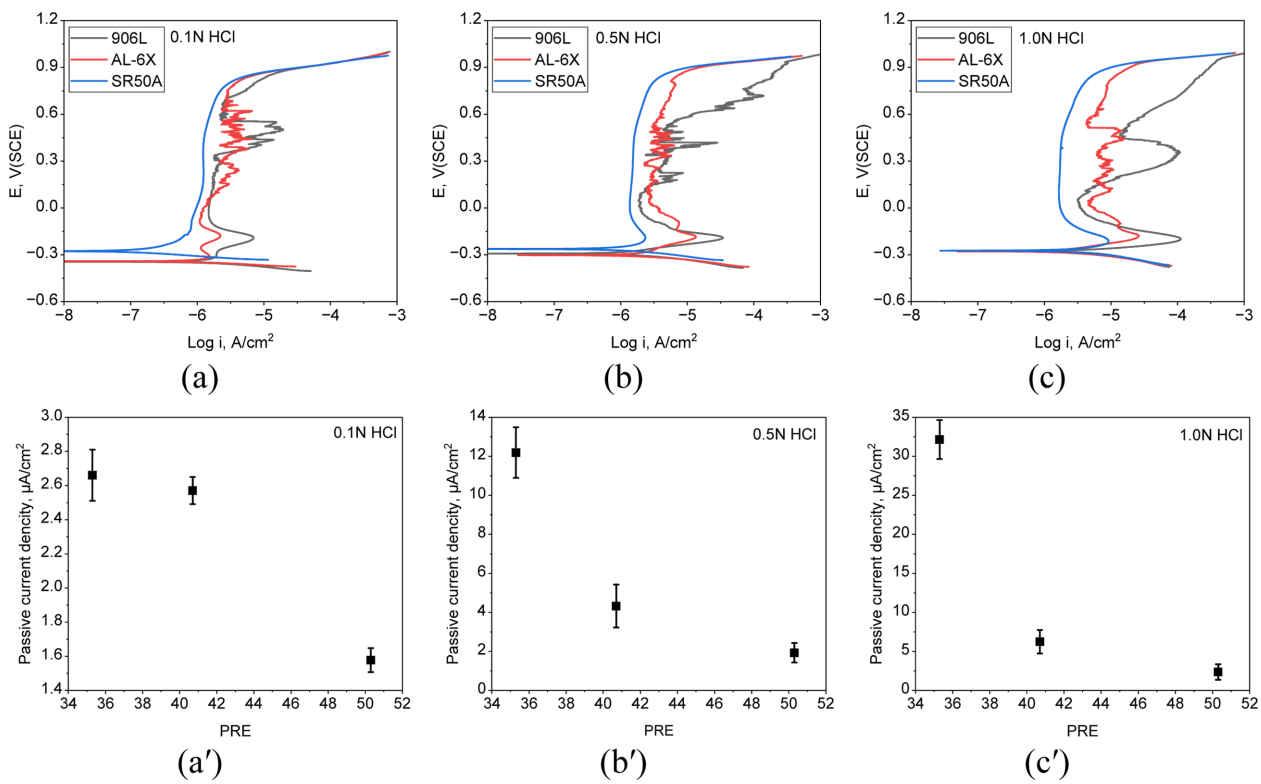

Fig. 1. Electrochemical polarization behavior(a-c) and passive current density(a′-c′) at +0.6 V(SCE) of austenitic stainless steels with different PRE values in deaerated HCl solutions at 25 °C; (a, a′) 0.1 N HCl, (b, b′) 0.5 N HCl, (c, c′) 1.0 N HCl

the passive current density measured at +0.6 V(SCE) (Fig. 1a′–c′) for austenitic stainless steels with different PRE values in deaerated 0.1, 0.5, and 1.0 N HCl solutions at 25 ºC. As shown in Fig. 1a–c, the passive current densities (i_p) in 0.1 N HCl solution (Fig. 1a) were measured as 0.71 μA/cm^2, 2.24 μA/cm^2, and 7.08 μA/cm^2 for 904L, AL-6X, and SR50A, respectively. This indicates that a higher PRE facilitates passive film formation and allows the alloys to reach a stable passive state at lower current densities. Although the pitting potentials were similar for all three alloys, a comparison of the current behavior within the passive region revealed that alloys with higher PRE values maintained more stable passive current densities. In 0.5 N HCl solution (Fig. 1b), the critical passive current densities of 904L, AL-6X, and SR50A increased to 2.34 μA/cm^2, 13.49 μA/cm^2, and 34.67 μA/cm^2, respectively. For 904L, the pitting potential appeared around 0.53 V(SCE), whereas no distinct pitting potential was observed for AL-6X and SR50A. Similarly, in 1.0 N HCl solution (Fig. 1c), the critical passive current densities increased to 9.23 μA/cm^2, 26.31 μA/cm^2, and 112.21 μA/cm^2 for 904L, AL-6X, and SR50A, respectively. Under this condition, only 904L exhibited an unstable pitting potential, while the two higher PRE alloys showed no evidence of pitting formation.

Fig. 1a′–c′ present the passive current densities measured at +0.6 V(SCE) as a function of PRE and HCl concentration for each alloy. In 0.1 N HCl (Fig. 1a′), the passive current densities for 904L (2.66 μA/cm^2) and AL-6X (2.57 μA/cm^2) were similar, while SR50A, with the highest PRE, exhibited the lowest value of 1.58 μA/cm^2. In 0.5 N HCl (Fig. 1b′), the current density of 904L increased sharply to approximately 12.19 μA/cm^2, while SR50A remained below 1.93 μA/cm^2, and AL-6X showed an intermediate value of 4.33 μA/cm^2. In 1.0 N HCl (Fig. 1c′), these differences became more pronounced, with 904L exhibiting a significantly higher current density of about 32.14 μA/cm^2, compared to 6.24 μA/cm^2 for AL-6X and below 2.36 μA/cm^2 for SR50A.

Fig. 2 shows the impedance behavior of passive films formed at +0.6 V(SCE) on austenitic stainless steels with different PRE values in deaerated HCl solutions at 25 ºC.

Fig. 2a–c show the Nyquist plots of passive films as a function of PRE. In 0.1 N HCl solution (Fig. 2a), all three alloys exhibited typical semicircular shapes, with the diameter increasing as the PRE value increased, indicating higher passive film resistance. In 0.5 N HCl (Fig. 2b), the semicircle diameter of 904L was significantly reduced, whereas AL-6X and SR50A still maintained large diameters. In 1.0 N HCl (Fig. 2c), both AL-6X and 904L showed smaller semicircles, while SR50A with the highest PRE retained a large diameter. For clarity, enlarged views of the semicircles corresponding to 904L are included in Fig. 2a–c.

Fig. 2a′–c′ present the Bode plots of passive films as a function of PRE. In 0.1 N HCl solution (Fig. 2a′), 904L exhibited low impedance and a reduced frequency response, whereas AL-6X and SR50A maintained relatively high impedance values. A similar trend was observed in 0.5 N HCl (Fig. 2b′), where 904L again showed low impedance, while AL-6X and SR50A retained higher values. In 1.0 N HCl (Fig. 2c′), 904L displayed a markedly low impedance, indicating a sharp decline in passive film stability, while SR50A maintained the highest value and AL-6X showed an intermediate response. These results demonstrate that, regardless of HCl concentration, 904L consistently exhibits unstable frequency responses, whereas higher PRE values contribute to maintaining passive film stability.

Fig. 2a″–c″ show the polarization resistance (R_p) of austenitic stainless steels with different PRE values. In 0.1 N HCl solution (Fig. 2a″), AL-6X and SR50A exhibited high R_p values of 879.3 × 10^3 Ω·cm^2 and 881.9 × 10^3 Ω·cm^2, respectively, whereas 904L showed a relatively low value of 433.1 Ω·cm^2. In 0.5 N HCl (Fig. 2b″), 904L again displayed the lowest R_p of 468.3 Ω·cm^2, while AL-6X and SR50A maintained high levels of 688.9 × 10^3 Ω·cm^2 and 778.2 × 10^3 Ω·cm^2, respectively. In 1.0 N HCl (Fig. 2c″), the differences became more pronounced: 904L dropped sharply to 109.2 Ω·cm^2, and AL-6X also decreased considerably to 24.49 × 10^3 Ω·cm^2, whereas SR50A retained a high R_p of 771.7 × 10^3 Ω·cm^2. These results indicate that, irrespective of HCl concentration, an increase in PRE leads to a significant improvement in passive film resistance, demonstrating superior corrosion resistance with higher PRE values [37,47,49,54-57].

Fig. 3 shows the Mott–Schottky behavior of passive films formed at +0.6 V(SCE) on austenitic stainless steels with different PRE values in deaerated HCl solutions at 25 ºC.

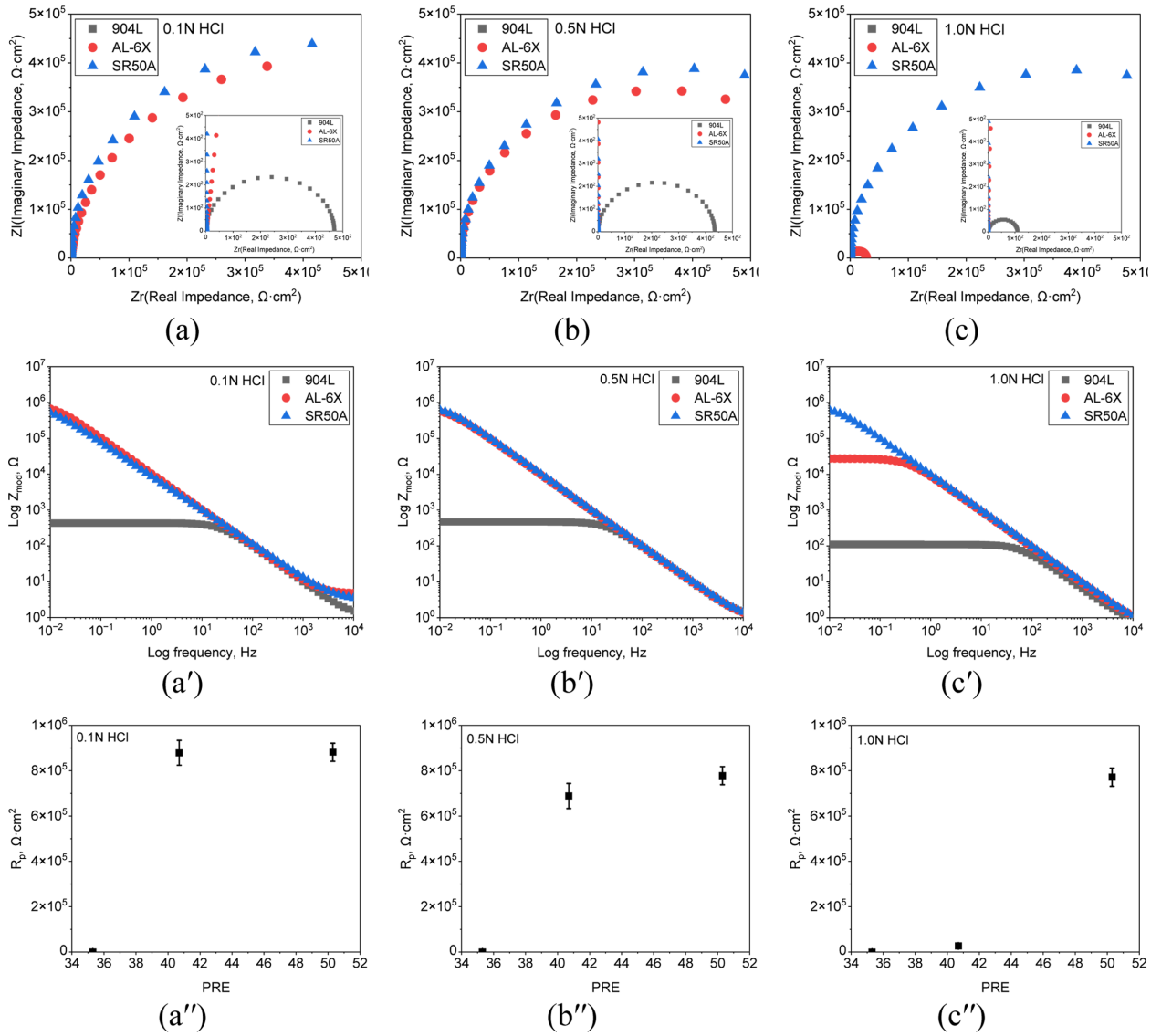

Fig. 2. Impedance behavior of passive films formed at +0.6 V(SCE) on austenitic stainless steels with different PRE values in deaerated HCl solutions at 25 °C: (a–c) Nyquist plots, (a′–c′) Bode plots, (a″–c″) polarization resistance (R_p); (a, a′, a″) 0.1 N HCl, (b, b′, b″) 0.5 N HCl, (c, c′, c″) 1.0 N HCl

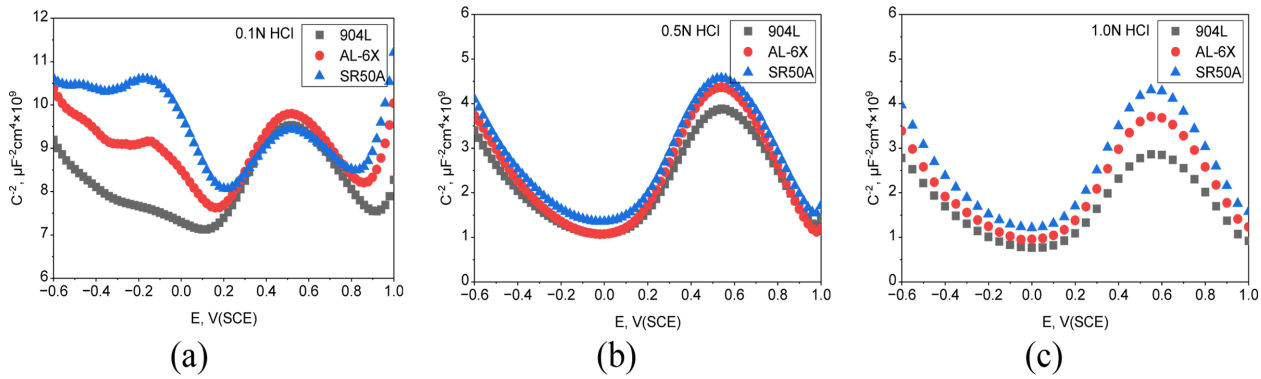

Fig. 3. Mott–Schottky plots of passive films formed at +0.6 V(SCE) on austenitic stainless steels with different PRE values in deaerated HCl solutions at 25 °C; (a) 0.1 N HCl, (b) 0.5 N HCl, (c) 1.0 N HCl

In 0.1 N HCl (Fig. 3a), p-type semiconductive behavior was observed in the potential range of −0.2 V(SCE) to +0.2 V(SCE), while n-type behavior appeared between +0.2 V(SCE) and +0.5 V(SCE). As the PRE increased, the slope corresponding to the p-type characteristics showed a gradual increase. In contrast, the n-type slopes of 904L and AL-6X were similar, whereas SR50A exhibited a relatively lower slope. In 0.5 N HCl (Fig. 3b), p-type semiconductive behavior was observed in the potential range of −0.6 V(SCE) to 0 V(SCE), while n-type behavior appeared between 0 V(SCE) and +0.5 V(SCE). The slope corresponding to the p-type characteristics increased slightly with PRE, with SR50A showing the highest value. Although the n-type slopes showed no significant differences among the alloys, SR50A exhibited a relatively higher value. Overall, under the 0.5 N HCl condition, the changes in slope with respect to PRE were not pronounced. In 1.0 N HCl (Fig. 3c), p-type semiconductive behavior was observed in the potential range of −0.6 V(SCE) to 0 V(SCE), while n-type behavior appeared between 0 V(SCE) and +0.5 V(SCE). The slope corresponding to the p-type characteristics clearly increased with higher PRE, with the most pronounced value observed for SR50A. The n-type slopes also showed a distinct increasing trend as PRE increased, making the slope variations most evident under the 1.0 N HCl condition. The flat band potential (E_{fb}), donor density (N_D), and acceptor density (N_A) obtained from these results are summarized in Table 2 [51-55].

Fig. 4 shows the total defect density of austenitic stainless steels with different PRE values as a function of HCl concentration. In 0.1 N HCl (Fig. 4a), the lowest PRE alloy 904L, exhibited the highest defect density of approximately 5.13×10^{28} cm^{-3}, while AL-6X and SR50A showed relatively lower values of 2.40×10^{28} cm^{-3} and 2.26×10^{28} cm^{-3}, respectively. In 0.5 N HCl (Fig. 4b), the overall defect densities of all three alloys decreased, with 904L, AL-6X, and SR50A recording 2.54×10^{28} cm^{-3}, 2.10×10^{28} cm^{-3}, and 2.02×10^{28} cm^{-3}, respectively, with SR50A showing the lowest value due to its higher PRE. A similar trend was observed in 1.0 N HCl (Fig. 4c), where the defect density decreased with increasing PRE: 904L exhibited 3.28×10^{28} cm^{-3}, AL-6X 2.67×10^{28} cm^{-3}, and SR50A 2.33×10^{28} cm^{-3}. These results indicate that higher PRE values reduce the charge carrier density within the passive film, thereby enhancing its stability.

Table 2. Donor density (N_D), acceptor density (N_A), and flat-band potential (E_{fb}) of passive films formed at +0.6 V(SCE) on austenitic stainless steels with different PRE values in deaerated HCl solutions at 25 °C

	0.1N HCl			0.5N HCl			1.0N HCl		
	904L	AL-6X	SR 50A	904L	AL-6X	SR 50A	904L	AL-6X	SR 50A
E_{fb} by P slope, V(SCE)	0.75	0.41	0.36	0.059	0.10	0.086	0.045	0.043	0.021
E_{fb} by N slope, V(SCE)	0.091	0.052	0.011	0.031	0.033	0.024	0.038	0.050	0.040
N_A (10^{28} cm^{-3})	4.16	1.43	0.91	1.52	1.21	1.16	1.85	1.60	1.40
N_D (10^{28} cm^{-3})	0.97	0.97	1.35	1.02	0.89	0.86	1.43	1.07	0.93

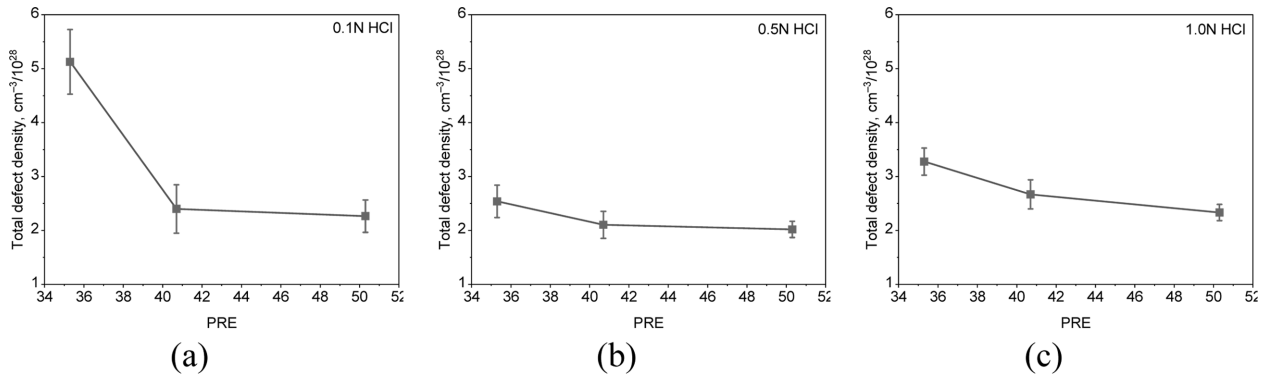

Fig. 4. Variation of total defect density of passive films on austenitic stainless steels with different PRE values (25 °C, deaerated, +0.6 V (SCE)); (a) 0.1 N HCl, (b) 0.5 N HCl, (c) 1.0 N HCl

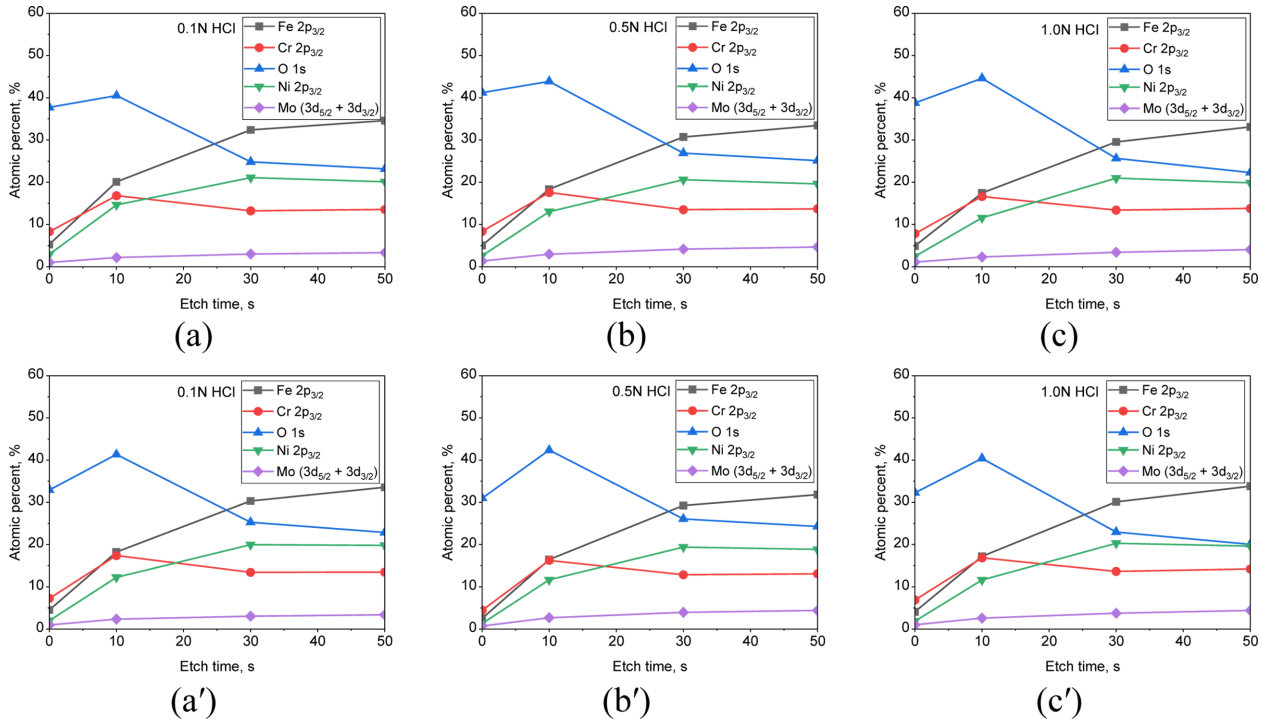

Fig. 5. XPS depth profiles of passive films formed for 2 h at +0.6 V(SCE) on austenitic stainless steels with different PRE values (25 °C, deaerated); (a, a′) 904L, (b, b′) AL-6X, (c, c′) SR50A; (a–c) 0.1 N HCl, (a′–c′) 1.0 N HCl

4. Discussion

Fig. 5 illustrates the XPS depth profiles of passive films formed at +0.6 V(SCE) on austenitic stainless steels with different PRE values. In both 0.1 N HCl (Fig. 5a–c) and 1.0 N HCl (Fig. 5a′–c′), compositional variations of Fe $2p_{3/2}$, Cr $2p_{3/2}$, O 1s, Ni $2p_{3/2}$, and Mo ($3d_{5/2}$ + $3d_{3/2}$) were observed as a function of depth. Regardless of alloy type or solution concentration, a general trend was evident in which the proportion of O 1s was higher in the outer layer, while the metallic components increased toward the inner layer. In addition, alloys with higher PRE values exhibited relatively stable distributions of Cr $2p_{3/2}$ and Mo ($3d_{5/2}$ + $3d_{3/2}$). Detailed distributions of the major elements under 0.1 N HCl and 1.0 N HCl conditions are further analyzed in Fig. 6 ~ 10 and Fig. 11 ~ 15 respectively.

Fig. 6 shows the depth distribution of Cr $2p_{3/2}$ species in the passive films of austenitic stainless steels with different PRE values. For Cr^M (Fig. 6a), the content tended to gradually increase toward the interior of the film, and the higher the PRE, the relatively lower the Cr^M content appeared. Cr_2O_3 (Fig. 6b) tended to decrease in depth, but its content was more stably maintained as PRE increased. $Cr(OH)_3$ (Fig. 6c) generally decreased along with depth direction and showed a similar distribution among the alloys regardless of PRE. CrO_4^{2-} (Fig. 6d) also decreased with depth, yet alloys with higher PRE contained it at higher levels. Notably, CrO_4^{2-} is recognized as a key factor related to the formation of a cation-selective outer layer in the bipolar model, and its stabilization becomes more pronounced with higher PRE, thereby enhancing the stability and corrosion resistance of the passive film. Overall, increasing PRE led to a more stable formation of Cr oxides, which represents an important factor contributing to improved durability and corrosion resistance of the passive film [21,22,24,41-43].

For Fe^M (Fig. 7a), relatively higher proportions were observed from the outer layer of the film in 904L and AL-6X, indicating that the metallic Fe content was more pronounced compared with SR50A. This suggests that alloys with lower PRE could not sufficiently stabilize Fe oxide formation within the passive film. For Fe^{2+} (Fig. 7b), AL-6X and SR50A showed similar variations, with contents gradually decreasing with depth, whereas 904L consistently exhibited relatively lower Fe^{2+} levels throughout the entire depth range, showing a clear

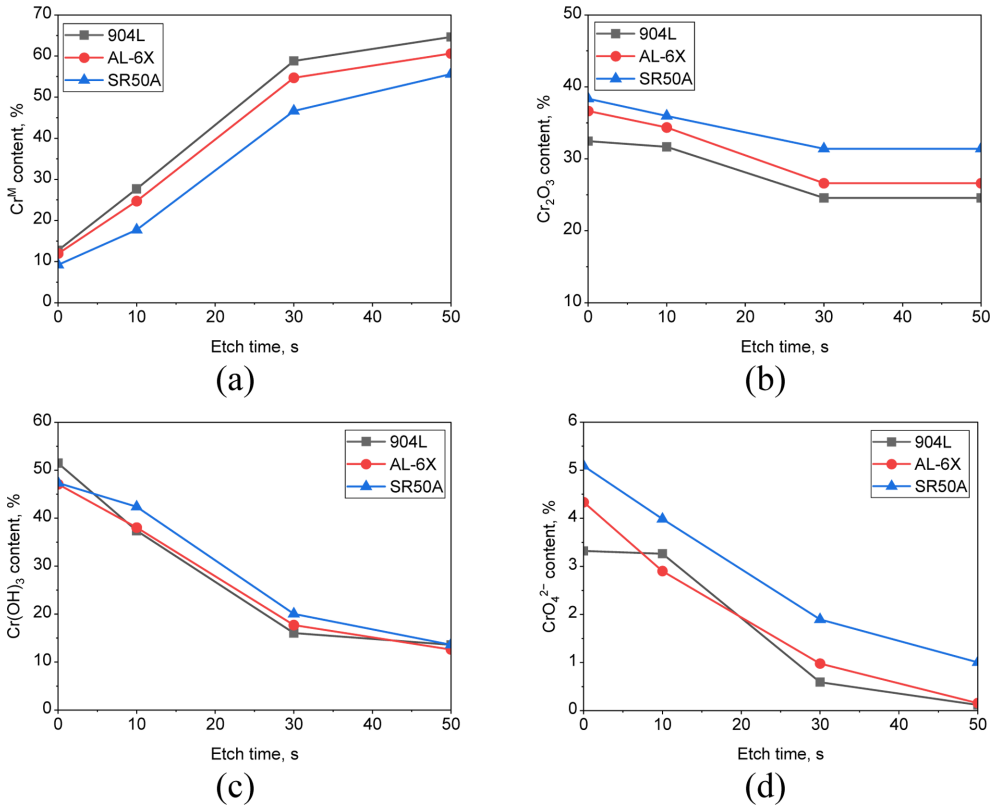

Fig. 6. Effect of PRE values on the depth distribution of Cr $2p_{3/2}$ species in the passive films formed for 2 h at +0.6 V(SCE) in 0.1 N HCl solution (25 °C, deaerated); (a) Cr^M, (b) Cr_2O_3, (c) $Cr(OH)_3$, (d) CrO_4^{2-}

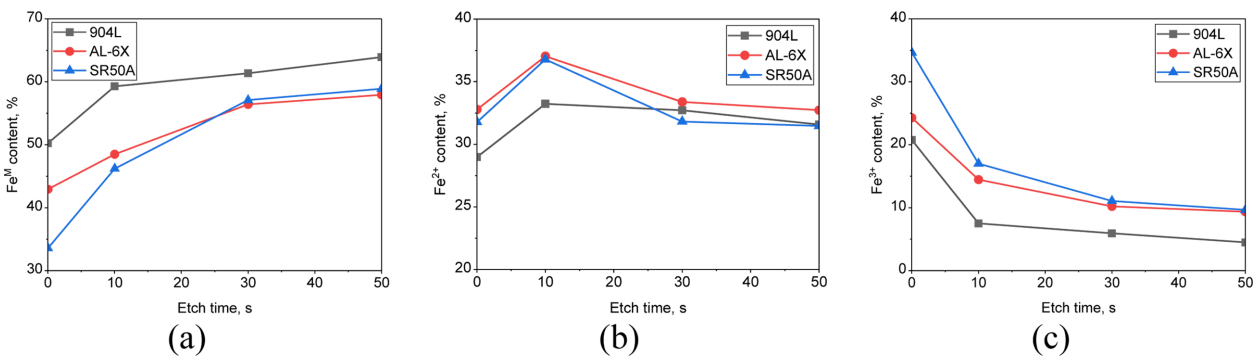

Fig. 7. Effect of PRE values on the depth distribution of Fe $2p_{3/2}$ species in the passive films formed for 2 h at +0.6 V(SCE) in 0.1 N HCl solution (25 °C, deaerated); (a) Fe^M, (b) Fe^{2+}, (c) Fe^{3+}

difference from the other alloys. For Fe^{3+} (Fig. 7c), a decreasing trend with depth was observed for all alloys; however, the higher the PRE, the more stably Fe^{3+} content was maintained. These results indicate that in alloys with lower PRE, the outer layer of the passive film is strongly influenced by Fe oxides, and the insufficient stabilization of the Fe oxide layer weakens the p-type characteristics, which accounts for the lower slopes observed in the Mott–Schottky analysis. In contrast, as PRE increases, a more balanced formation between Fe oxides in the outer layer and Cr oxides in the inner layer leads to a stabilized bilayer structure, thereby enhancing the corrosion resistance of the passive film [31-33,42,46].

Fig. 8 shows the depth distribution of O 1s species within the passive film. For O^{2-} (Fig. 8a), the content increased toward the interior of the film, which is

associated with the formation of a stable oxide layer, although no significant differences were observed among the alloys. OH^- (Fig. 8b) exhibited a high proportion in the outer layer and sharply decreased toward the interior, indicating that hydroxide species play a relatively important role in the outer layer. H_2O (Fig. 8c) maintained an overall low level, primarily confined to the outer layer, and rapidly diminished in the interior, demonstrating that adsorbed water molecules are present in the outer region. Overall, O^{2-} contributes to the formation of the inner oxide layer, whereas OH^- and H_2O are predominantly distributed in the outer layer. These results suggest that oxygen species are key factors distinguishing the composition of the inner and outer layers of the passive film. However, no clear correlation with PRE was identified [31,36,42,50].

Fig. 9 shows the depth distribution of Mo ($3d_{5/2}$ + $3d_{3/2}$) species in the passive film. For Mo^M (Fig. 9a), the content

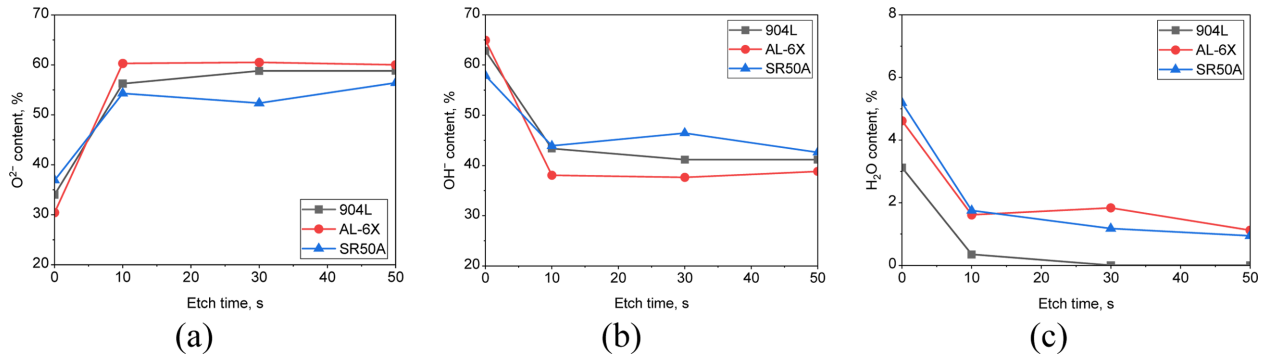

Fig. 8. Effect of PRE values on the depth distribution of O 1s species in the passive films formed for 2 h at +0.6 V(SCE) in 0.1 N HCl solution (25 °C, deaerated); (a) O^{2-}, (b) OH^-, (c) H_2O

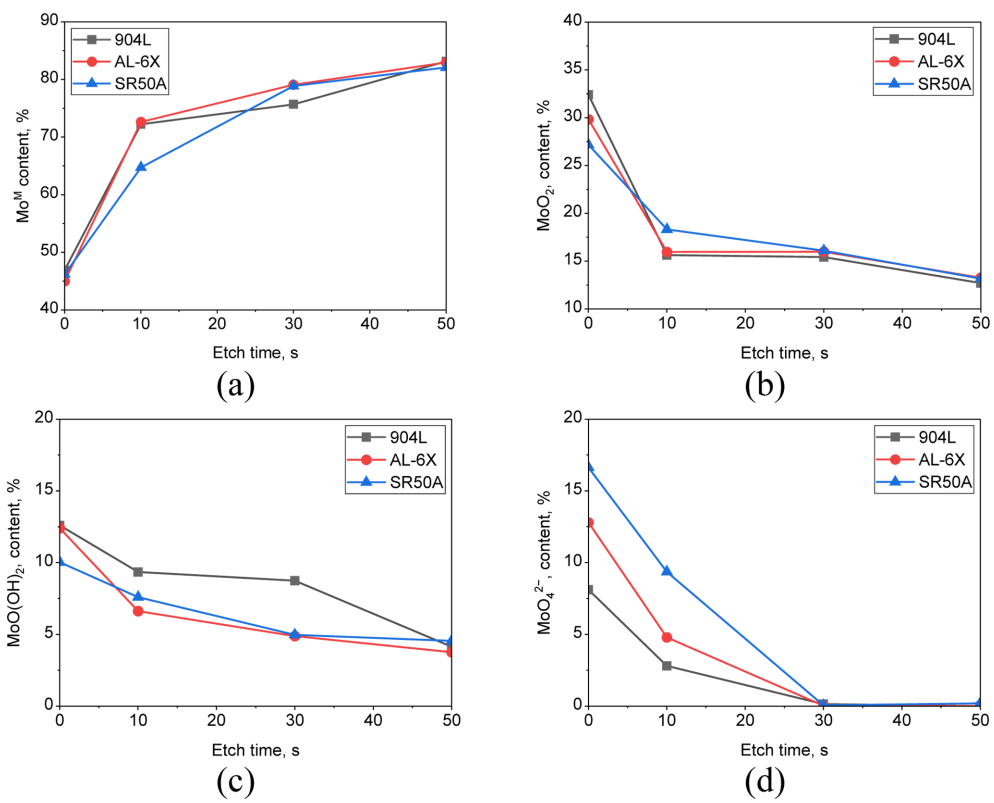

Fig. 9. Effect of PRE values on the depth distribution of Mo ($3d_{5/2}$ + $3d_{3/2}$) species in the passive films formed for 2 h at +0.6 V(SCE) in 0.1 N HCl solution (25 °C, deaerated); (a) Mo^M, (b) MoO_2, (c) $MoO(OH)_2$, (d) MoO_4^{2-}

increased toward the interior of the film, indicating that metallic Mo was distinctly present in the region close to the metal substrate. MoO_2 (Fig. 9b) exhibited a relatively high content in the outer layer but decreased sharply toward the interior, confirming that the oxide state formed at the surface tended to lose its stability as it progressed inward. $MoO(OH)_2$ (Fig. 9c) showed a clear fraction in the outer layer but continuously decreased toward the interior, indicating that hydroxide-type Mo was mainly distributed in the outer region. MoO_4^{2-} (Fig. 9d) was observed as the most dominant species in the outer layer, and its proportion remained relatively high, particularly in alloys with higher PRE. This suggests that MoO_4^{2-} contributes to the stabilization of the passive film by enhancing the cation-selective nature of the outer layer, thereby suppressing cation transport and improving corrosion resistance, as described by the bipolar model [20-23,25,44,45].

Fig. 10 shows the depth distribution of Ni $2p_{3/2}$ species in the passive film. For Ni^M (Fig. 10a), the content tended to decrease with increasing PRE, indicating that metallic Ni was more prevalent at the surface in alloys with lower PRE. In contrast, NiO (Fig. 10b) gradually increased with higher PRE, suggesting that Ni oxides were more stably formed in alloys with higher PRE [30,32,33,50].

Fig. 11 shows the depth distribution of Cr $2p_{3/2}$ species in the passive films of austenitic stainless steels with different PRE values in 1.0 N HCl solution. For Cr^M (Fig. 11a), the content gradually increased toward the interior of the film, with all three alloys showing a similar distribution level. Cr_2O_3 (Fig. 11b) continuously decreased with depth, and no distinct differences were observed among the alloys regardless of PRE. $Cr(OH)_3$ (Fig. 11c) also showed a decreasing tendency with depth, and the distribution differences among the alloys were not significant. In contrast, CrO_4^{2-} (Fig. 11d) exhibited a clear distribution difference depending on PRE. The higher the PRE, the relatively higher the fraction of CrO_4^{2-} maintained in the outer layer, which acted as a key factor in strengthening the passive film by providing a cation-selective property in the outer region. These results demonstrate that CrO_4^{2-} plays an important role in improving corrosion resistance even under high-concentration HCl conditions. In summary, under the 1.0 N HCl condition, Cr^M, Cr_2O_3, and $Cr(OH)_3$ showed no significant differences among the alloys, whereas CrO_4^{2-} exhibited a distinct distribution depending on PRE, indicating that higher PRE enhances the stability of the Cr oxide layer [21,22,24,41-43].

Fig. 12 shows the depth distribution of Fe $2p_{3/2}$ species in the passive films of austenitic stainless steels with different PRE values in 1.0 N HCl solution. Fe^M (Fig. 12a) and Fe^{3+} (Fig. 12c) exhibited similar tendencies in all alloys regardless of PRE, showing general distributions that gradually increased or decreased with depth. In contrast, Fe^{2+} (Fig. 12b) was distributed at relatively higher fractions in alloys with lower PRE, showing a distinct difference. Therefore, under the 1.0 N HCl condition, Fe species overall did not show a clear difference depending on PRE, although Fe^{2+} was present at relatively higher levels in alloys with lower PRE [31-33,42,46].

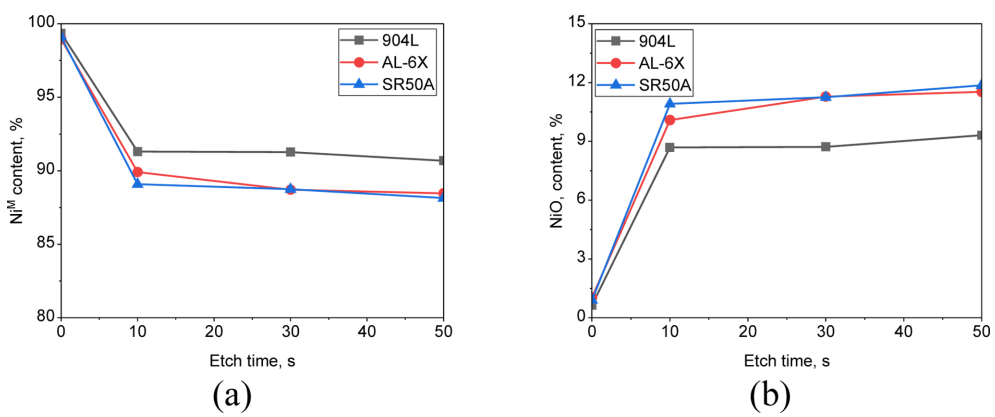

Fig. 10. Effect of PRE values on the depth distribution of Ni $2p_{3/2}$ species in the passive films formed for 2 h at +0.6 V(SCE) in 0.1 N HCl solution (25 °C, deaerated); (a) Ni^M, (b) NiO

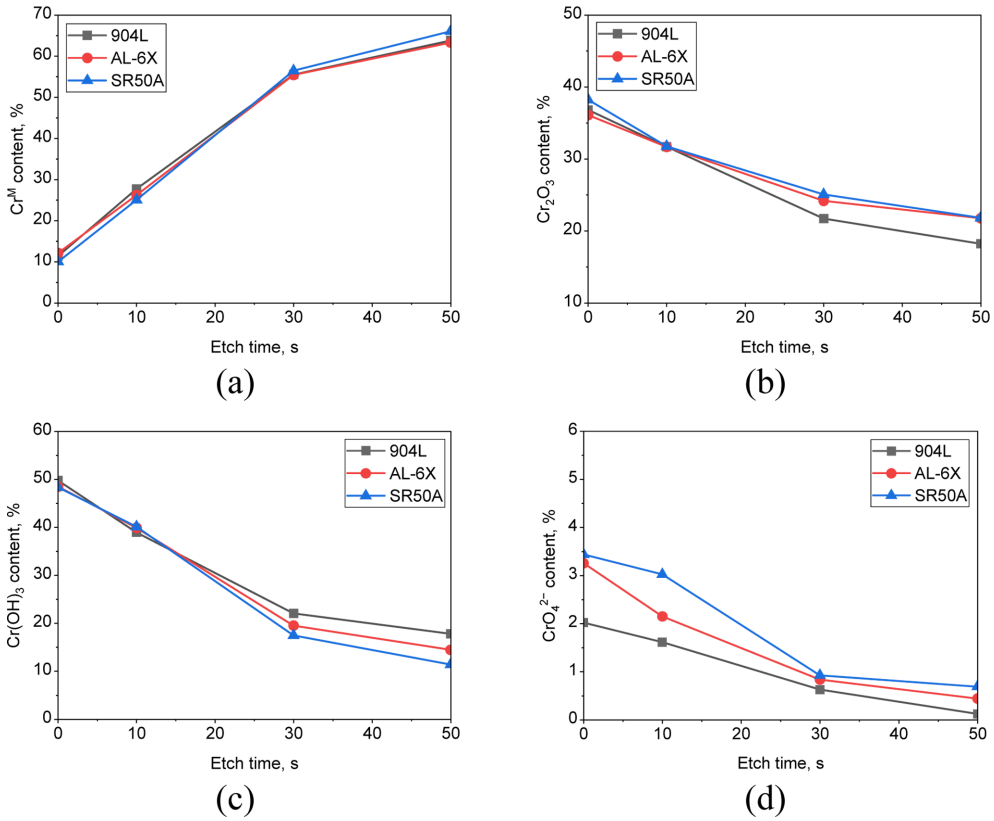

Fig. 11. Effect of PRE values on the depth distribution of Cr $2p_{3/2}$ species in the passive films formed for 2 h at +0.6 V(SCE) in 1.0 N HCl solution (25 °C, deaerated); (a) Cr^M, (b) Cr_2O_3, (c) $Cr(OH)_3$, (d) CrO_4^{2-}

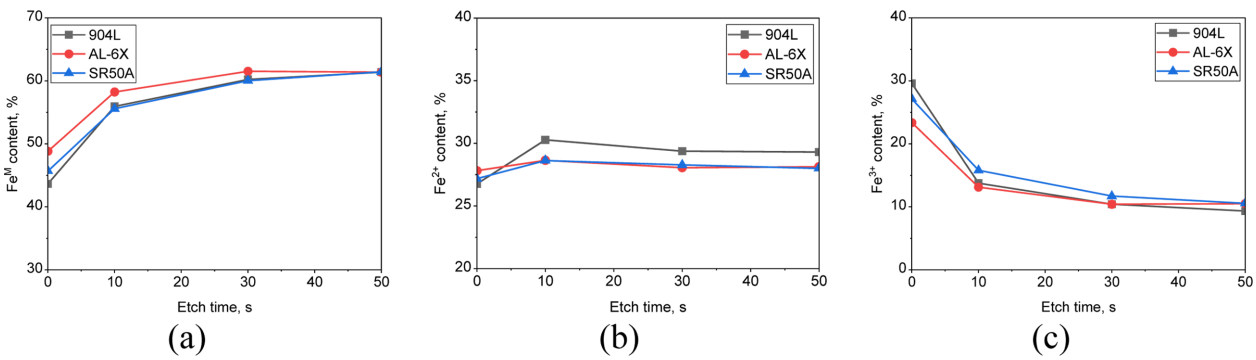

Fig. 12. Effect of PRE values on the depth distribution of Fe $2p_{3/2}$ species in the passive films formed for 2 h at +0.6 V(SCE) in 1.0 N HCl solution (25 °C, deaerated); (a) Fe^M, (b) Fe^{2+}, (c) Fe^{3+}

Fig. 13 shows the depth distribution of O 1s species in the passive films of austenitic stainless steels with different PRE values in 1.0 N HCl solution. O^{2-} (Fig. 13a) distinctly increased toward the interior of the film and was maintained at relatively higher levels in SR50A with higher PRE. In contrast, AL-6X showed lower fractions across the entire depth range, while 904L exhibited intermediate levels, showing no strong PRE dependence. OH^- (Fig. 13b) was dominant in the outer layer and sharply decreased toward the interior. SR50A exhibited the lowest values, while 904L maintained an intermediate level between SR50A and AL-6X. H_2O (Fig. 13c) remained at overall low levels and was mainly distributed in the outer layer. The lowest content was observed in 904L, whereas AL-6X showed the highest fraction, with SR50A at an intermediate level. In summary, under the

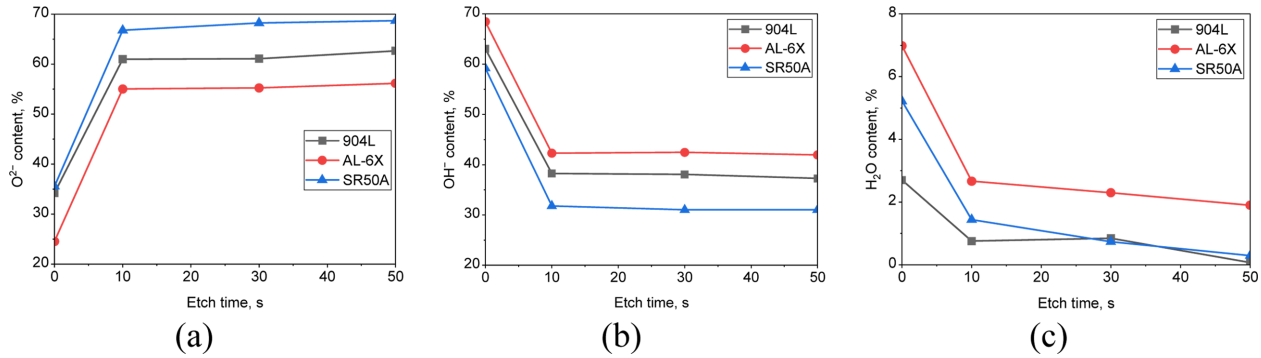

Fig. 13. Effect of PRE values on the depth distribution of O 1s species in the passive films formed for 2 h at +0.6 V(SCE) in 1.0 N HCl solution (25 °C, deaerated); (a) O^{2-}, (b) OH^{-}, (c) H_2O

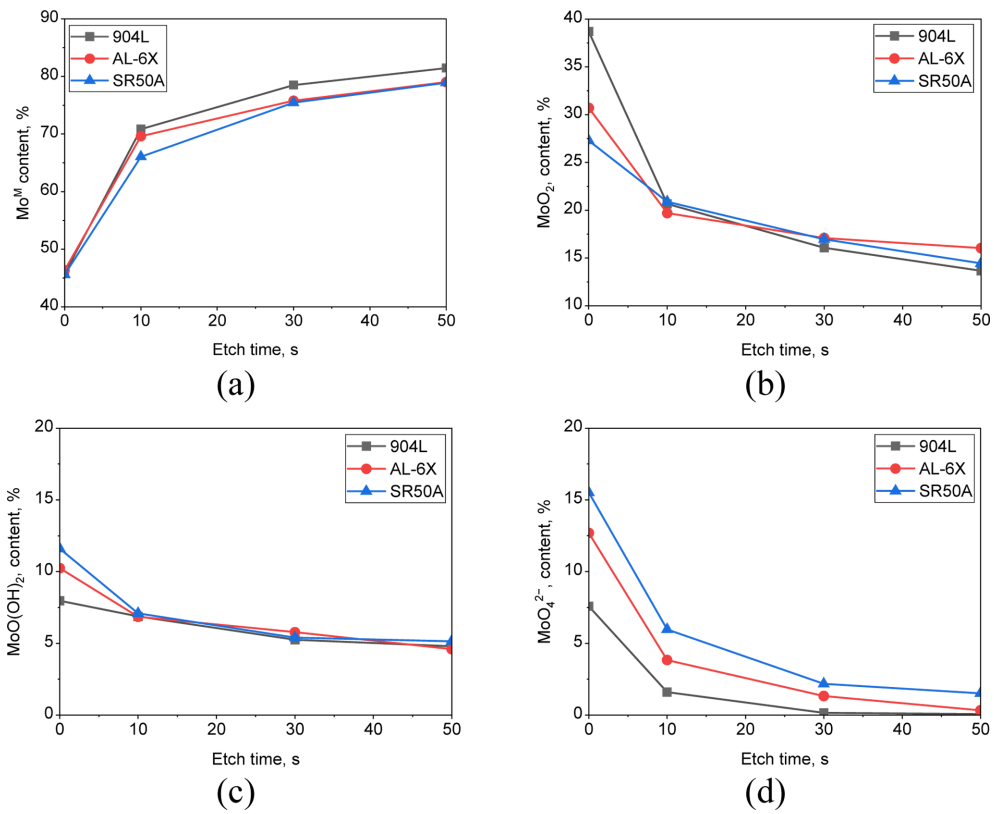

Fig. 14. Effect of PRE values on the depth distribution of Mo ($3d_{5/2}$ + $3d_{3/2}$) species in the passive films formed for 2 h at +0.6 V(SCE) in 1.0 N HCl solution (25 °C, deaerated); (a) Mo^{M}, (b) MoO_2, (c) $MoO(OH)_2$, (d) MoO_4^{2-}

1.0 N HCl condition, SR50A showed relatively higher O^{2-} and lower OH^{-} / H_2O, indicating a more stable oxide layer, whereas AL-6X exhibited lower O^{2-} and higher H_2O, suggesting a larger contribution of hydrated species in the outer layer. 904L presented intermediate characteristics between the two alloys.

Fig. 14 shows the depth distribution of Mo ($3d_{5/2}$ + $3d_{3/2}$) species in the passive films of austenitic stainless steels with different PRE values in 1.0 N HCl solution. Mo^{M} (Fig. 14a) increased toward the interior of the film and appeared at relatively higher fractions in 904L with lower PRE. MoO_2 (Fig. 14b) was mainly observed at higher fractions in the outer layer, but its content gradually decreased as PRE increased. Toward the inner layer, the differences among the alloys were not significant. $MoO(OH)_2$ (Fig. 14c) showed a clear fraction in the outer

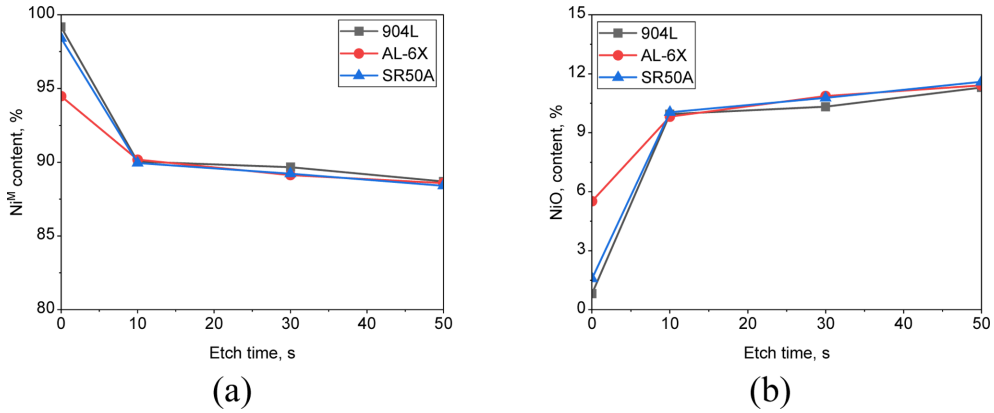

Fig. 15. Effect of PRE values on the depth distribution of Ni $2p_{3/2}$ species in the passive films formed for 2 h at +0.6 V(SCE) in 1.0 N HCl solution (25 °C, deaerated); (a) Ni^M, (b) NiO

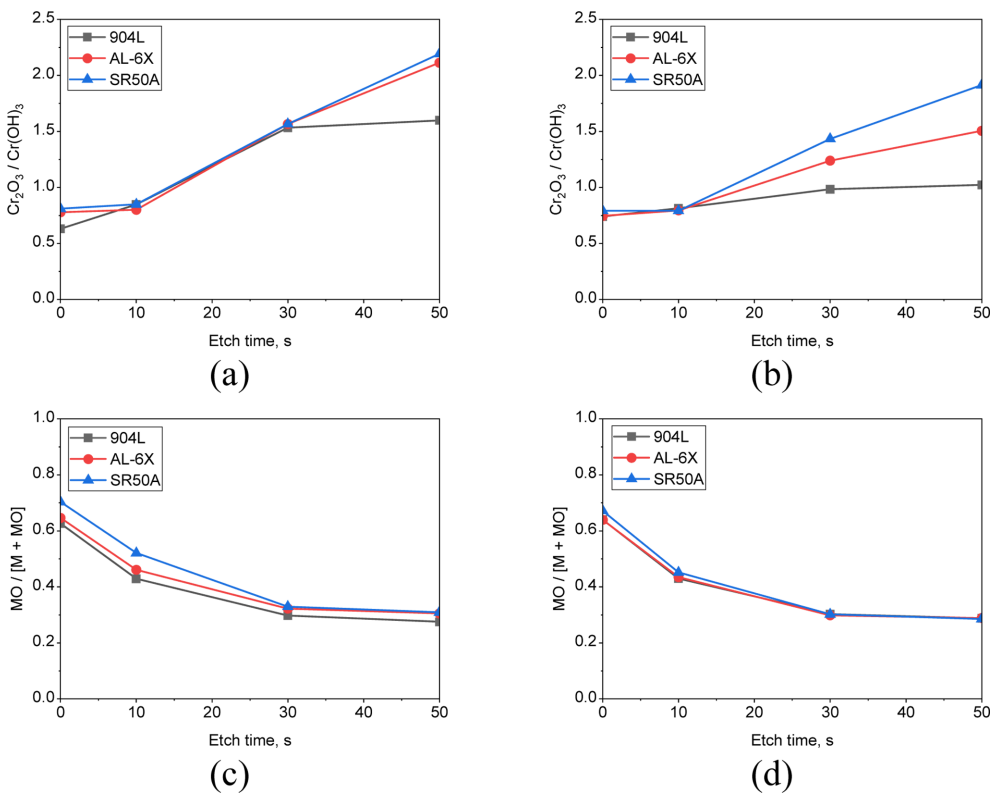

Fig. 16. Effect of PRE values on the Cr_2O_3 / $Cr(OH)_3$ ratio and MO / (M + MO) ratio in the passive films formed for 2 h at +0.6 V(SCE) in HCl solutions (25 °C, deaerated): (a) Cr_2O_3 / $Cr(OH)_3$ ratio in 0.1 N HCl, (b) Cr_2O_3 / $Cr(OH)_3$ ratio in 1.0 N HCl, (c) MO / (M + MO) ratio in 0.1 N HCl, (d) MO / (M + MO) ratio in 1.0 N HCl (MO means metal oxide)

layer but sharply decreased with depth, and alloys with higher PRE exhibited relatively higher fractions in the outer layer, while the differences diminished toward the inner layer. MoO_4^{2-} (Fig. 14d) was identified as the most dominant species in the outer layer, and its fraction remained the highest in SR50A with higher PRE. This indicates that, as described by the bipolar model, MoO_4^{2-} plays a key role in enhancing the stability and corrosion resistance of the passive film by promoting cation selectivity in the outer layer and suppressing cation transport. In other words, with increasing PRE, MoO_4^{2-} and $MoO(OH)_2$ were reinforced in the outer layer, whereas MoO_2 tended to decrease [20-23,25,44,45].

Fig. 15 shows the depth distribution of Ni $2p_{3/2}$ species

in the passive films of austenitic stainless steels with different PRE values in 1.0 N HCl solution. Ni^{M} (Fig. 15a) exhibited the highest fraction in the outer layer and gradually decreased toward the interior of the film. No significant differences were observed among the alloys, and no clear influence of PRE was identified. NiO (Fig. 15b) showed relatively low values in the outer layer but gradually increased with depth. Similarly, differences among the alloys were not significant, and no direct correlation with PRE was observed.

Fig. 16 shows the ratios of Cr_2O_3 / $Cr(OH)_3$ and MO / (M + MO) in the passive films of austenitic stainless steels in HCl solutions. The Cr_2O_3 / $Cr(OH)_3$ ratio exhibited a gradual increase toward the interior of the film in both 0.1 N HCl (Fig. 16a) and 1.0 N HCl (Fig. 16b). Notably, SR50A with the highest PRE maintained the highest values, whereas AL-6X and 904L showed relatively lower levels. This indicates that stable oxides such as Cr_2O_3 accumulate more effectively in alloys with higher PRE. Meanwhile, the MO / (M + MO) ratio showed a decreasing trend toward the interior of the film in both 0.1 N HCl (Fig. 16c) and 1.0 N HCl (Fig. 16d). In 904L with the lowest PRE, the ratio remained low even from the outer layer, whereas SR50A and AL-6X showed relatively higher initial values, which diminished with depth. Overall, as PRE increased, the Cr_2O_3 / $Cr(OH)_3$ ratio increased significantly, while the MO / (M + MO) ratio decreased, indicating that the passive films tend to form more stable oxide-rich layers in alloys with higher PRE [56,57].

During XPS depth profiling, partial reduction of oxides or selective removal of oxygen may occur during the Ar^{+} ion sputtering process, which could partially affect the relative composition of Fe and O elements. However, since all samples were analyzed under identical conditions, this is not expected to significantly impact comparative trends between alloys. These limitations of XPS depth profiling are considered to warrant further research.

Fig. 17 shows the change in the bipolar index of the passive film as a function of the PRE value. The bipolar index was derived by summing the absolute values of the p-type slope and the n-type slope, following a method proposed in previous studies [58], considering that the passive film is divided into an inner layer and an outer

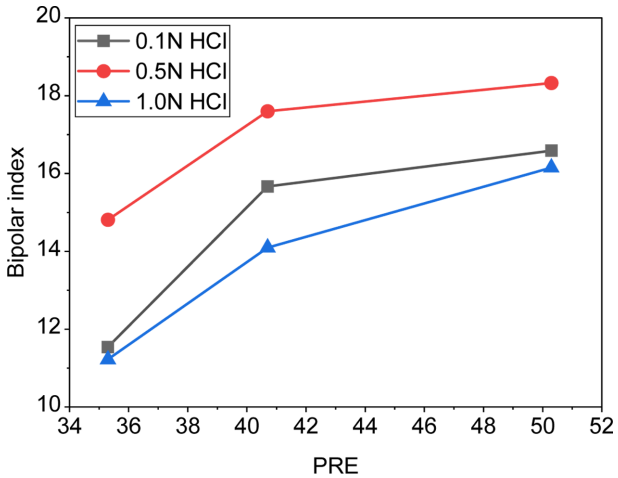

Fig. 17. Effect of PRE on the bipolar index of the passive films formed at +0.6 V(SCE) in deaerated HCl solutions at 25 °C

layer, each exhibiting p-type and n-type semiconductor characteristics, respectively. This definition does not mathematically express the semiconductor characteristics resulting from the addition of alloying elements but rather uses an empirical correlation to describe the combined characteristics of the two semiconductor tendencies. As a result, the bipolar index showed a clear increasing trend with higher PRE under all HCl concentration conditions. This indicates that in alloys with higher PRE, the oxide components formed in the inner and outer layers are more balanced, thereby enhancing both p-type and n-type semiconductive properties simultaneously. In other words, the bipolar index serves as a quantitative indicator reflecting the stable development of the bilayer structure of the passive film and becomes a key factor in explaining the correlation between PRE and corrosion resistance.

Fig. 18 shows the relationship between the bipolar index and corrosion-related parameters of the passive film (passive current density and polarization resistance) as a function of HCl concentration. Regarding the relationship with i_p, in 0.1 N HCl (Fig. 18a), i_p showed a slight decrease with increasing bipolar index, although the overall variation was not significant. In 0.5 N HCl (Fig. 18b), i_p clearly decreased as the bipolar index increased, with a sharp drop observed in the higher bipolar index range. A similar trend was observed in 1.0 N HCl (Fig. 18c), where i_p rapidly decreased with increasing bipolar index, indicating that a higher bipolar index is closely associated with lower passive current density. The relationship with

R_p showed similar behavior. In 0.1 N HCl (Fig. 18a′), R_p increased with higher bipolar index, while in 0.5 N HCl (Fig. 18b′), a more pronounced increase was observed. In 1.0 N HCl (Fig. 18c′), R_p increased sharply with increasing bipolar index, confirming that alloys with a higher bipolar index exhibit significantly enhanced resistance of the passive film. Consequently, the bipolar index showed an inverse relationship with i_p and a direct relationship with R_p.

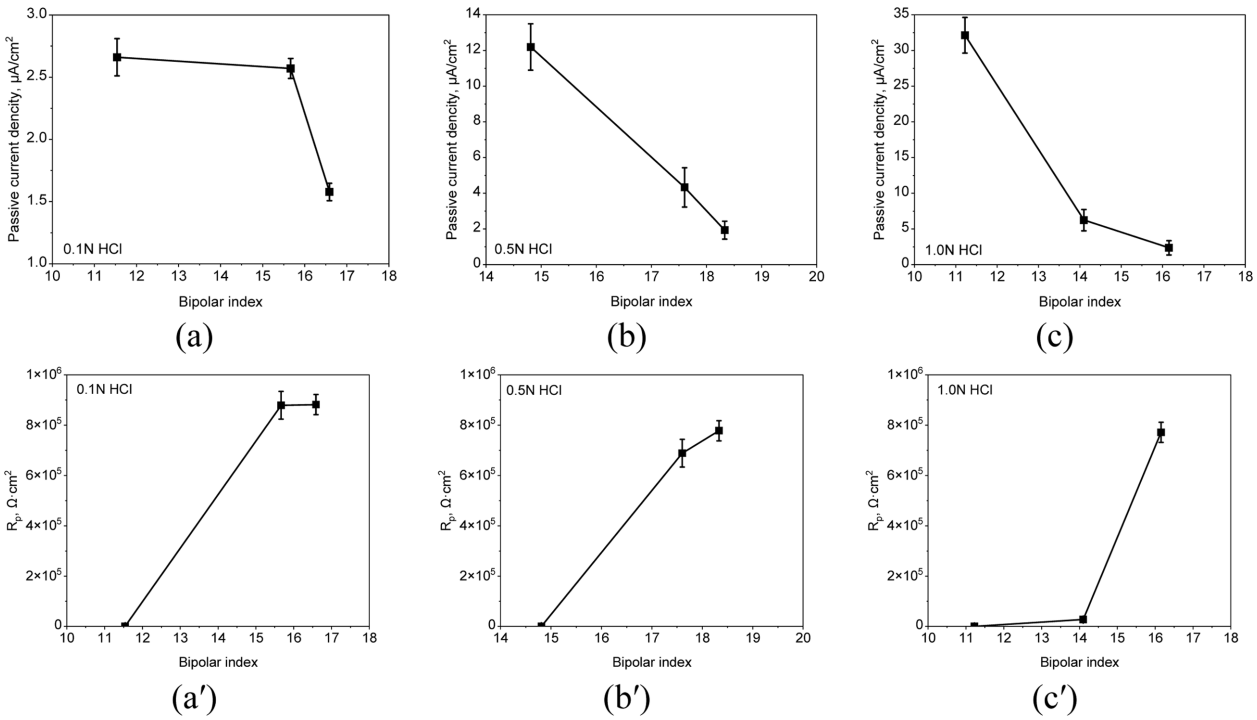

Fig. 18. Relationship between bipolar index and corrosion parameters of the passive films formed at +0.6 V(SCE) in deaerated HCl solutions at 25 °C: (a–c) passive current density (i_p), (a′–c′) polarization resistance (R_p); (a, a′) 0.1 N HCl, (b, b′) 0.5 N HCl, (c, c′) 1.0 N HCl

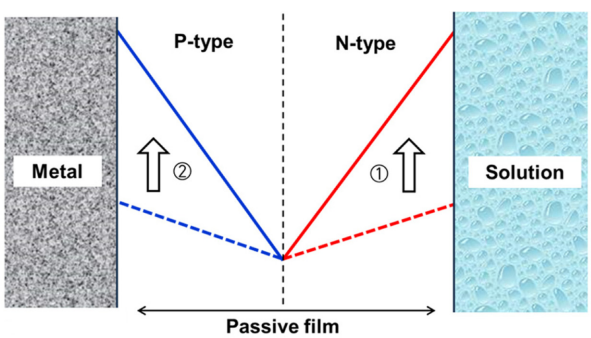

Increasing PRE of the alloy,

N-type property of the passive film

- MeO_4^{2-} (CrO_4^{2-}, MoO_4^{2-}) increase → N-type slope ↑

P-type property of the passive film

- Cr_2O_3 / $Cr(OH)_3$ ratio increase → P-type slope ↑

Therefore

- Higher PRE → Bipolar Index ↑ → ip ↓, Rp ↑ → Corrosion resistance improved

Fig. 19. Schematic of the advanced bipolar model, illustrating how increasing the PRE number strengthens the passive film

This indicates that as the p-type and n-type characteristics of the passive film develop in a more balanced manner, the stability and corrosion resistance of the film are significantly enhanced. Therefore, the bipolar index can be regarded as an important parameter for both PRE-based alloy design and the evaluation of passive film characteristics.

In this study, a new model was proposed to solve the limitations of the conventional bipolar model, as illustrated in Fig. 19. Fig. 19 schematically represents the effect of increasing PRE elements (Cr, Mo) on the p-type and n-type characteristics of the passive film. With higher PRE contents, the distribution of MeO_4^{2-} oxyanions such as CrO_4^{2-} and MoO_4^{2-} in the outer layer markedly increased, inducing changes in the electronic structure of the outer layer and resulting in an increase in the n-type slope observed in Mott–Schottky analysis. In addition, as PRE increased, the Cr_2O_3 / $Cr(OH)_3$ ratio in the inner layer increased, with a particularly pronounced contribution from Cr_2O_3. This led to structural stabilization of the inner layer and, consequently, an increase in the p-type slope. In other words, these complementary changes, with simultaneous strengthening of the n-type characteristics in the outer layer and the p-type characteristics in the inner layer, explain the observed increase in the bipolar index (|p-type slope| + |n-type slope|) with higher PRE, which proposed by our group [58]. The increase in the bipolar index decreased the passive current density (i_p) and increased the polarization resistance (R_p), which ultimately led to a reduction in the total defect density in the passive film.

5. Conclusions

In this study, the electrochemical and semiconductive behavior of passive films on austenitic stainless steels with different PRE values was investigated in deaerated HCl solutions, and the advanced bipolar model of the passive film was proposed. The main conclusions are as follows.

(1) With increasing PRE, the distribution of oxyanion species (MeO_4^{2-}), in the outer layer increased, enhancing the structural stability and cation selectivity of the outer layer. As a result, alloys with higher PRE exhibited an increasing trend in n-type characteristics of the outer layer.

(2) As PRE increased, the Cr_2O_3 / $Cr(OH)_3$ ratio in the inner layer markedly increased. The greater proportion of Cr_2O_3 contributed to the stabilization of the inner layer structure, resulting in an increasing tendency in p-type slope.

(3) These complementary changes in the outer and inner layers led to a bilayer structure in which both p-type and n-type characteristics were simultaneously enhanced. Consequently, the bipolar index (|p-type slope| + |n-type slope|) increased with higher PRE. As the bipolar index increased, the passive current density (i_p) decreased, the polarization resistance (R_p) increased, and the total defect density within the passive film decreased. As a result, the corrosion resistance of the alloys was significantly improved.

Acknowledgments

This research was supported by the “Research Fund of Gyeongkuk National University” and “Grant number 2025–2026”. The authors would like to acknowledge the valuable support provided by Dr. S. N. Kim for his assistance with the XPS analysis.

References

1. F. L. LaQue and H. R. Copson, *Corrosion resistance of metal and alloys*, *2nd ed*., p. 375, Reinhold, New York (1963).
2. I. Olefjord, The passive state of stainless steels, *Materials Science and Engineering*, **42**, 161 (1980). Doi: https://doi.org/10.1016/0025-5416(80)90025-7
3. A. Hannani, F. Kermiche, A. Pourbaix, and K. Belmokre, Characterisation of passive film on AISI304 stainless steel, *Transactions of the IMF*, **75**, 7 (1997). Doi: https://doi.org/10.1080/00202967.1997.11871135
4. S. Haupt and H. H. Strehblow, A combined surface analytical and electrochemical study of the formation of passive layers on alloys in 0.5 M H_2SO_4, *Corrosion Science*, **37**, 43 (1995). Doi: https://doi.org/10.1016/0010-938x(94)00104-e
5. J. Ruijing, Y. Wang, X. Wen, C. Chen, and J. Zhao, Effect of time on the characteristics of passive film formed on stainless steel, *Applied Surface Science*, **412**, 214 (2017). Doi: https://doi.org/10.1016/j.apsusc.2017.03.155
6. M. Benoit, C. Bataillon, B. Gwinner, F. Miserque, M. E. Orazem, C. M. Sánchez-Sánchez, B. Tribollet, and V. Vivier, Comparison of different methods for measuring

the passive film thickness on metals, *Electrochimica Acta*, **201**, 340 (2016). Doi: https://doi.org/10.1016/j.electacta.2015.12.173
7. H. H. Uhlig and R. W. Revie, *Corrosion and corrosion control*, p. 69, John Wiley and Sons, Hoboken, USA (1985).
8. R. Kirchheim, B. Heine, H. Fischmeister, S. Hofmann, H. Knote, and U. Stolz, The passivity of iron-chromium alloys, *Corrosion Science*, **29**, 899 (1989). Doi: https://doi.org/10.1016/0010-938X(89)90060-7
9. M. Tsukada, H. Adachi, and C. Satoko, Theory of electronic structure of oxide surfaces, *Progress in Surface Science*, **14**, 113 (1983). Doi: https://doi.org/10.1016/0079-6816(83)90001-1
10. A. T. Fromhold Jr. and J. Kruger, Space-charge and concentration-gradient effects on anodic oxide film formation, *Journal of The Electrochemical Society*, **120**, 722 (1973). Doi: https://doi.org/10.1149/1.2403545
11. N. Sato, An overview on the passivity of metals, *Corrosion Science*, **31**, 1 (1990). Doi: https://doi.org/10.1016/0010-938X(90)90086-K
12. A. M. P. Simões, M. G. S. Ferreira, B. Rondot, and M. da Cunha Belo, Study of passive films formed on AISI 304 stainless steel by impedance measurements and photoelectrochemistry, *Journal of The Electrochemical Society*, **137**, 82 (1990). Doi: https://doi.org/10.1149/1.2086444
13. V. Maurice, W. P. Yang, and P. Marcus, X-ray photoelectron spectroscopy and scanning tunneling microscopy study of passive films formed on (100) Fe-18Cr-13Ni single-crystal surfaces, *Journal of The Electrochemical Society*, **145**, 909 (1998). Doi: https://doi.org/10.1149/1.1838366
14. P. Marcus and M. E. Bussell, XPS study of the passive films formed on nitrogen-implanted austenitic stainless steels, *Applied Surface Science*, **19**, 7 (1992). Doi: https://doi.org/10.1016/0169-4332(92)90163-R
15. E. De Vito and P. Marcus, XPS study of passive films formed on molybdenum-implanted austenitic stainless steels, *Surface and Interface Analysis*, **19**, 403 (1992). Doi: https://doi.org/10.1002/sia.740190175
16. G. Lorang, M. da Cunha Belo, A. M. P. Simões, and M. G. S. Ferreira, Chemical composition of passive films on AISI 304 stainless steel, *Journal of The Electrochemical Society*, **141**, 3347 (1994). Doi: https://doi.org/10.1149/1.2059338
17. R. B. Soares, W. R. C. Campos, P. L. Gastelois, W. A. A. Macedo, L. F. P. Dick, and V. F. C. Lins, Electrochemical properties of passive film formed on super martensitic stainless steel in a chloride medium, *Corrosion*, **76**, 884 (2020). Doi: https://doi.org/10.5006/3230
18. T. P. Hoar, D. C. Mears, and G. P. Rothwell, The relationships between anodic passivity, brightening and pitting, *Corrosion Science*, **5**, 279 (1965). Doi: https://doi.org/10.1016/S0010-938X(65)90614-1
19. D. D. Macdonald, Passivity the key to our metals-based civilization, *Pure and Applied Chemistry*, **71**, 951 (1999). Doi: https://doi.org/10.1351/pac199971060951
20. M. Sakashita and N. Sato, The effect of molybdate anion on the ion-selectivity of hydrous ferric oxide films in chloride solutions, *Corrosion Science*, **17**, 473(1977). Doi: https://doi.org/10.1016/0010-938X(77)90003-8
21. M. Sakashita and N. Sato, Ion-selectivity of nickel chromate, molybdate, and tungstate precipitate membranes, *Denki Kagaku Oyobi Kogyo Butsuri Kagaku*, **44**, 395 (1976). Doi: https://doi.org/10.5796/kogyobutsurikagaku.44.395
22. M. Sakashita and N. Sato, Ion selectivity of precipitate films affecting passivation and corrosion of metals, *Corrosion*, **35**, 351 (1979). Doi: https://doi.org/10.5006/0010-9312-35.8.351
23. C. R. Clayton and Y. C. Lu, A bipolar model of the passivity of stainless steel: The role of Mo addition, *Journal of The Electrochemical Society*, **133**, 2465 (1986). Doi: https://doi.org/10.1149/1.2108451
24. A. R. Brooks, C. R. Clayton, K. Doss, and Y. C. Lu, On the role of Cr in the passivity of stainless steel, *Journal of The Electrochemical Society*, **133**, 2459 (1986). Doi: https://doi.org/10.1002/chin.198714025
25. C. R. Clayton and Y. C. Lu, A bipolar model of the passivity of stainless steels—III. The mechanism of MoO42− formation and incorporation, *Corrosion Science*, **29**, 881 (1989). Doi: https://doi.org/10.1016/0010-938X(89)90059-0
26. Y. S. Kim, Y. S. Park, A study on effects of Mo addition on the corrosion resistance of stainless steels, *Journal of the Corrosion Science Society of Korea*, **18**, 67 (1989). https://www.j-cst.org/opensource/pdfjs/web/pdf_viewer.htm?code=J00180200067
27. Y. S. Kim and Y. S. Park, A study on effects of N addition on the passivating mechanism of stainless steels, *Journal of the Corrosion Science Society of Korea*, **18**, 97 (1989). https://www.j-cst.org/opensource/pdfjs/web/pdf_viewer.htm?code=J00180200097
28. A. Fattah-alhosseini, Passivity of AISI 321 stainless steel in 0.5 M H_2SO_4 solution studied by Mott–Schottky anal-

ysis in conjunction with the point defect model, *Arabian Journal of Chemistry*, **9**, S1342 (2016). Doi: https://doi.org/10.1016/j.arabjc.2012.02.015

29. E. A. Cho and H. S. Kwon, A study on the electronic properties of passive film formed on Fe-20Cr by photoelectrochemical and Mott-Schottky analysis, *Corrosion Science and Technology*, **31**, 275 (2002). https://www.j-cst.org/opensource/pdfjs/web/pdf_viewer.htm?code=C00010400275
30. T. Ohtsuka, M. Ueda, and M. Abe, Aging of passive oxide on SUS304 stainless steel in a sulfuric acid solution, *Journal of The Electrochemical Society*, **163**, C459 (2016). Doi: https://doi.org/10.1149/2.0721608jes
31. M. Ma, C. He, H. Liu, and L. Chen, Influence of cerium and tungsten addition on the passive behaviour of 444-type ferritic stainless steels, *International Journal of Electrochemical Science*, **14**, 2277 (2019). Doi: https://doi.org/10.20964/2019.03.31
32. Y. Yue, C. Liu, and M. Jiang, Evolution of passive film on 304 stainless steel during nitric acid passivation, *Steel Research International*, **93**, 2200026 (2022). Doi: https://doi.org/10.1002/srin.202200026
33. M. G. S. Ferreira, N. E. Hakiki, G. Goodlet, S. Faty, A. M. P. Simões, and M. da Cunha Belo, Influence of the temperature of film formation on the electronic structure of oxide films formed on 304 stainless steel, *Electrochimica Acta*, **46**, 3767 (2001). Doi: https://doi.org/10.1016/S0013-4686(01)00658-2
34. A. Fattah-alhosseini and S. Vafaeian, Comparison of the electrochemical behavior between coarse-grained and fine-grained AISI 430 ferritic stainless steel by Mott–Schottky analysis and EIS measurements, *Journal of Alloys and Compounds*, **639**, 301 (2015). Doi: https://doi.org/10.1016/j.jallcom.2015.03.142
35. H. Zhang, J. Zhao, C. Yang, M. Shen, X. Zhang, T. Xi, L. Yin, H. Zhao, X. Liu, L. Liu, et al., Corrosion resistance of Cu-bearing 316L stainless steel tuned by various passivation potentials, *Surface abd Interface Analysis*, **53**, 592 (2021). Doi: https://doi.org/10.1002/sia.6946
36. I. H. Toor, M. Ejaz, and H. S. Kwon, Mott–Schottky analysis of passive films on Cu-containing Fe–20Cr–xCu (x = 0, 4) alloys, *Corrosion Engineering Science and Technology: The International Journal of Corrosion Processes and Corrosion Control*, **49**, 390 (2014). Doi: https://doi.org/10.1179/1743278214Y.0000000154
37. M. A. Ameer, A. M. Fekry, and F. E. Heakal, Electrochemical behaviour of passive films on molybdenum-containing austenitic stainless steels in aqueous solutions, *Electrochimica Acta*, **50**, 43 (2004). Doi: https://doi.org/10.1016/j.electacta.2004.07.011
38. K. Osozawa and H. J. Engell, The anodic polarization curves of iron–nickel–chromium alloys, *Corrosion Science*, **6**, 389 (1966). Doi: https://doi.org/10.1016/S0010-938X(66)80022-7
39. K. Hashimoto, K. Asami, A. Kawashima, H. Habazaki, and E. Akiyama, The role of corrosion-resistant alloying elements in passivity, *Corrosion Science*, **49**, 42 (2007). Doi: https://10.1016/j.corsci.2006.05.003
40. J. Chen and J. K. Wu, The improved passivation of iron induced by additions of tungsten, *Corrosion Science*, **30**, 53 (1990). Doi: https://doi.org/10.1016/0010-938X(90)90234-V
41. Z. Wang, E.-M. Paschalidou, A. Seyeux, S. Zanna, V. Maurice, and P. Marcus, Mechanisms of Cr and Mo enrichments in the passive oxide film on 316L austenitic stainless steel, *Frontiers in Materials*, **6**, 232 (2019). Doi: https://doi.org/10.3389/fmats.2019.00232
42. T. Ohtsuka, M. Abe, and T. Ishii, The effect of impurity concentration and Cr content on the passive oxide films in ferritic stainless steels, *Journal of The Electrochemical Society,* **162**, C528 (2015). Doi: https://doi.org/10.1149/2.0621510jes
43. C. O. A. Olsson and D. Landolt, Passive films on stainless steels—Chemistry, structure and growth, *Electrochimica Acta*, **48**, 1093 (2003). Doi: https://doi.org/10.1016/S0013-4686(02)00841-1
44. V. Maurice, H. Peng, L. H. Klein, A. Seyeux, S. Zanna, and P. Marcus, Effects of molybdenum on the composition and nanoscale morphology of passivated austenitic stainless steel surfaces, *Faraday Discussions*, **180**, 151 (2015). Doi: https://doi.org/10.1039/C4FD00231H
45. A. Pardo, M. C. Merino, A. E. Coy, F. Viejo, R. Arrabal, and E. Matykina, Effect of Mo and Mn additions on the corrosion behaviour of AISI 304 and 316 stainless steels in H_2SO_4, *Corrosion Science*, **50**, 780 (2008). Doi: https://10.1016/j.corsci.2007.11.004
46. A. Pardo, M. C. Merino, A. E. Coy, F. Viejo, R. Arrabal, and E. Matykina, Pitting corrosion behaviour of austenitic stainless steels – combining effects of Mn and Mo additions, *Corrosion Science*, **50**, 1796 (2008). Doi: https://10.1016/j.corsci.2008.04.005
47. J. Fan and Q. Zhang, Influence of molybdenum as alloying element on corrosion resistance of stainless steel rebar in simulated concrete pore solution with different pH, *International Journal of Electrochemical Science*, **15**,

7624 (2020). Doi: https://doi.org/10.20964/2020.08.10

48. D. D. Liang, X. S. Wei, C. T. Chang, J. W. Li, Y. Wang, X. M. Wang, and J. Shen, Effects of W addition on the electrochemical behaviour and passive film properties of Fe-based amorphous alloys in acetic acid solution, *Acta Metallurgica Sinica*, **31**, 1098 (2018). Doi: https://doi.org/10.1007/s40195-018-0791-8
49. D. Kim, S. Kim, J. Park, D.-I. Kim, B.-H. Shin, and J.-H. Yoon, Effects of passivation with Cu and W on the corrosion properties of super duplex stainless steel PRE 42, *Metals*, **14**, 284 (2024). Doi: https://doi.org/10.3390/met14030284
50. J. S. Kim, P. J. Xiang, and K. Y. Kim, Effect of tungsten and nickel addition on the repassivation behavior of stainless steel, *Corrosion*, **61**, 174 (2005). Doi: https://10.5006/1.3278172
51. ASTM G5-2004, Standard reference test method for making potentiostatic and potentiodynamic anodic polarization measurements, ASTM International, West Conshohocken, PA (2004).
52. N. N. Khobragade, A. V. Bansod, A. P. Patil, and M. Bihade, Effect of various ratios of nitric acid–chloride on electronic properties of passive films on AISI 304L stainless steel, *International Journal of Materials Research*, **109**, 522 (2018). Doi: https://doi.org/10.3139/146.111641
53. A. Fattah-alhosseini, M. A. Sonamia, A. Loghmani, and F. Z. Shoja, Passivity of AISI 316L stainless steel as a function of nitric concentration, *Journal of Advanced Materials and Processing*, **2**, 21 (2014). article_551653_19ada117a6162b235173428ec90bdc25.pdf
54. A. Fattah-Alhosseini, H. Aghamohammadi, and A. B. Safa, Electrochemical behavior assessment of Alloy 22 (UNS N06022) in hydrochloric acid solutions by electrochemical impedance spectroscopy and Mott–Schottky analyses, *Analytical & Bioanalytical Electrochemistry*, **7**, 728 (2015). https://www.magiran.com/p1489787
55. A. Fattah-alhosseini, H. Farahani, and O. Imantalab, The effect of solution concentration on the electrochemical behaviour of AISI 321 stainless steel in sulfuric solutions, *International Journal of Iron & Steel Society of Iran*, **9**, 19 (2012). https://journal.issiran.com/article_6536_9379c23ac12dc94053207373040bc791.pdf
56. S. H. Choi, Y. R. Yoo, and Y. S. Kim, Semiconductive tendency of the passive film formed on super austenitic stainless steel SR-50A in acidic or alkaline chloride solutions, *Crystals*, **14**, 766 (2024). Doi: https://doi.org/10.3390/cryst14090766
57. S. H. Choi, Y. R. Yoo, and Y. S. Kim, Dynamic variation in the semiconductive tendency of the passive film on duplex stainless steel in corrosion environments, *Materials*, **17**, 5963 (2024). Doi: https://doi.org/10.3390/ma17235963
58. S. H. Choi, Y. R. Yoo, Y. S. Kim, and Y. C. Kim, Effect of Cr, Mo, and W contents on the semiconductive properties of passive film of ferritic stainless steels, *Crystals*, **15**, 1097 (2025). Doi: https://doi.org/10.3390/cryst15091097